

# Spin-controlled superconductivity and tunable triplet correlations in graphene nanostructures

Klaus Halterman,<sup>1,\*</sup> Oriol T. Valls,<sup>2,†</sup> and Mohammad Alidoust<sup>3,‡</sup>

<sup>1</sup>Michelson Lab, Physics Division, Naval Air Warfare Center, China Lake, California 93555

<sup>2</sup>School of Physics and Astronomy, University of Minnesota, Minneapolis, Minnesota 55455

<sup>3</sup>Department of Physics, Norwegian University of Science and Technology, N-7491 Trondheim, Norway

(Dated: July 26, 2018)

We study graphene ferromagnet/superconductor/ferromagnet (F/S/F) nanostructures via a microscopic self-consistent Dirac Bogoliubov-de Gennes formalism. We show that as a result of proximity effects, experimentally accessible spin switching phenomena can occur as one tunes the Fermi level  $\mu_F$  of the F regions or varies the angle  $\theta$  between exchange field orientations. Superconductivity can then be switched on and off by varying either  $\theta$  or  $\mu_F$  (a spin-controlled superconducting graphene switch). The induced equal-spin triplet correlations in S can be controlled by tuning  $\mu_F$ , effectively making a graphene based two-dimensional spin-triplet valve.

PACS numbers: 74.45.+c, 72.80.Vp, 68.65.Pq, 81.05.ue

**Introduction.**—The continual development of graphene has sparked vast research efforts linked to emerging nanotechnologies that span numerous scientific disciplines. With its 2D hexagonal lattice structure and linear energy dispersion at low energies, graphene possesses many desirable properties [1–3], such as extremely high electrical conductivity, tensile strength, and thermal conductivity. Graphene has played a prominent part in recent significant advances involving transistors, solar cells, and tunable THz electromagnetic radiation detection [4]. Although graphene is intrinsically a gapless semiconductor, it can become superconducting (SC) as well as acquire ferromagnetic (FM) properties through doping or defects [3, 5]. Thus, with the existing capability to create hybrid structures involving FM and SC graphene, researchers are now seeking breakthroughs involving graphene-based low temperature spintronic devices. The effectiveness of a graphene spin valve or switch involving both ferromagnet (F) and superconductor (S) elements in contact is based on proximity effects, which dictate the behavior of both the singlet and triplet pairing correlations in each region [6–11]. In graphene, as opposed to most conventional materials, the Fermi level can be tuned via a gate potential. This leads to many practical SC device applications, e.g., the supercurrent in a nonmagnetic Josephson junction can be reversed by tuning the gate voltage [9].

In this Letter, we demonstrate that pairing correlations in F/S/F graphene structures can be experimentally modulated in a controllable way by changing either the relative magnetization direction or by manipulating the Fermi level  $\mu_F$  of the F layers, leading to new possibilities for graphene-based devices. We show that by tuning  $\mu_F$  (which can be done e.g. by applying an external electric field), a new type of spin switching can occur where the system transitions between a resistive normal state and a SC one. This spin switching is closely linked to the magnitude of the exchange interaction in the F layers: in FM graphene the exchange field,  $h$ , shifts the Dirac points for spin-up and spin-down quasiparticles by an amount  $-h$  and  $+h$  respectively. This shift can create an effective barrier for the electrons and holes, and its existence relates to spin dependent Klein tunneling [2, 3]. We find also that

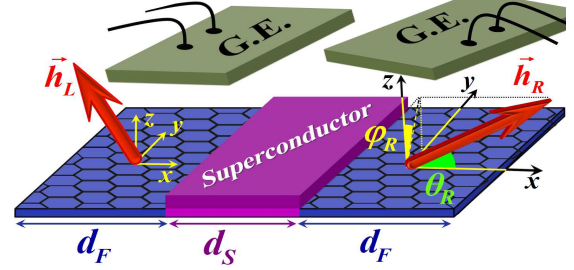


FIG. 1. (Color online) F/S/F geometry investigated. The magnetic structure is described by exchange fields  $\vec{h}_L$  and  $\vec{h}_R$  in the left and right magnets respectively. Their orientation is given by angles  $\theta_{L,R}$  and  $\varphi_{L,R}$ :  $\vec{h}_{L,R} = h_{L,R}(\cos \theta_{L,R}, \sin \theta_{L,R} \sin \varphi_{L,R}, \sin \theta_{L,R} \cos \varphi_{L,R})$ . The Fermi level in the F regions can be tuned via the gate electrodes (G.E.). The system is infinite in the  $x$ - $y$  plane.  $x$  is normal to the interfaces.

similar transitions between the resistive and SC states can be realized by variation the relative angle between the field orientations of the two F regions. In the graphene F/S/F system studied, equal-spin triplets can arise and be utilized as an effective triplet spin transistor: for certain exchange field configurations, the amount of equal-spin pairs in the superconductor can be controlled by the Fermi levels in the ferromagnets.

**Method.**—To study these phenomena, we have developed a microscopic self-consistent Dirac Bogoliubov-de Gennes (DBdG) approach to characterize graphene-based systems involving  $s$ -wave superconductors and ferromagnets with general exchange field orientations and tunable Fermi levels. We also computed the critical temperature of a F/S/F nanostructure from the linearized[12] self consistency equation. The confinement of the massless Dirac fermions along the  $x$  direction in Fig. 1 requires boundary conditions compatible with the DBdG equations. As in the famously difficult infinite potential well problem in relativistic quantum mechanics [13], the vanishing of the wavefunction at the outer boundaries of a quasi-1D “box” becomes problematic and alternate approaches are needed to avoid manifestations of the Klein paradox [2]. Several approaches are possible. The one we

take here (analogous to methods used in the study of the “bag model”) incorporates in the Hamiltonian terms corresponding to fictitious additional layers in the outer regions beyond the studied system [13, 14].

The inclusion of magnetism into the DBdG Hamiltonian yields the following  $16 \times 16$  Hamiltonian where  $\pm$ -signs refer to the graphene valleys,  $K(+)$  and  $K'(-)$  [8–11]:

$$\begin{pmatrix} \mathcal{H}_M - \mu\hat{I} & \Delta(\vec{r})\hat{I} \\ \Delta^*(\vec{r})\hat{I} & -(\mathcal{T}\mathcal{H}_M\mathcal{T}^{-1} - \mu\hat{I}) \end{pmatrix} \Psi_n = \epsilon_n \Psi_n, \quad (1)$$

$$\mathcal{H}_M = \mathcal{H} \otimes \sigma_0 - \sigma_0 \otimes \vec{h}_{L,R} \cdot \vec{\sigma}, \quad \mathcal{H} = \begin{pmatrix} \mathcal{H}^+ & 0 \\ 0 & \mathcal{H}^- \end{pmatrix},$$

where  $\hat{I}$  is the  $8 \times 8$  identity matrix,  $\mu$  the chemical potential, and  $\mathcal{T}$  the time reversal operator. The  $1 \times 16$  wavefunction is  $\Psi_n \equiv (\Psi_{u,n}^\uparrow, \Psi_{u,n}^\downarrow, \Psi_{v,n}^\downarrow, \Psi_{v,n}^\uparrow)$ , with  $\Psi_{u,n}^\sigma \equiv (u_{n,A,K}^\sigma, u_{n,B,K}^\sigma, u_{n,A,K'}^\sigma, u_{n,B,K'}^\sigma)$ , and  $\Psi_{v,n}^\sigma \equiv (v_{n,A,K'}^\sigma, v_{n,B,K'}^\sigma, v_{n,A,K}^\sigma, v_{n,B,K}^\sigma)$ , with  $\epsilon_n$  being the Dirac fermions eigenenergies. The labels  $A$  and  $B$  denote the two sublattices that arise from the honeycomb lattice structure. The chemical potential takes the value  $\mu_F$  in the two magnets and  $\mu_S$  in the superconductor. The time-reversal operator in our chosen basis is given by  $\mathcal{T} = [\sigma_z \otimes \sigma_x \otimes (-i\sigma_y)]\mathcal{C}$ , where  $\mathcal{C}$  is the complex conjugation operator.  $\mathcal{H}^\pm$  is written succinctly as  $\mathcal{H}^\pm = v_F(\sigma_x p_x \pm \sigma_y p_y) + v_F^2 M(x)\sigma_z$ . Here  $\sigma_i$  are the  $2 \times 2$  Pauli matrices acting in sublattice space,  $\sigma_0$  the  $4 \times 4$  identity matrix, and  $v_F$  is the Fermi velocity in graphene. We have introduced, to avoid the previously mentioned Klein paradox [2, 13] problems, a mass term  $M(x)$  [11] which vanishes in the F/S/F region studied and is effectively infinite in two computationally added outer regions adjacent to the F portions [14]. The exchange fields,  $\vec{h}_{L,R}$ , in the left ( $L$ ) and right ( $R$ ) F electrodes can be of different magnitude and have different orientation angles (see Fig. 1). We will present results here only for the case where  $\phi_{L,R} = \pi/2$ ,  $\theta_R = 0$  and equal magnitudes,  $h_L = h_R \equiv h$ .

The coupling of electrons in a given valley with the hole excitations in the other one is accomplished through the  $s$ -wave pair potential  $\Delta(x)$  [11], and is determined self-consistently by  $\Delta(x) = g/2 \sum_{n,\lambda,\beta} (u_{n,\lambda,\beta}^\uparrow v_{n,\lambda,\beta}^{\downarrow*} + u_{n,\lambda,\beta}^\downarrow v_{n,\lambda,\beta}^{\uparrow*}) \tanh(\epsilon_n/2T)$ , where  $\lambda$  represents the sublattice index ( $A$  or  $B$ ),  $\beta$  the valley index ( $K$  or  $K'$ ), and  $T$  the system temperature. The coupling parameter,  $g$ , is a constant finite only in the superconductor region. The sum is restricted to those quantum states with positive energies below a “Debye” energy cutoff,  $\omega_D$ . With the quantization axis aligned along the  $z$  direction, the triplet amplitudes,  $f_{0,z}$  and  $f_{1,z}$ , can be written as  $f_{0,z} = 1/2 \sum_n (f_n^{\uparrow\downarrow} - f_n^{\downarrow\uparrow})\zeta_n(t)$ , and  $f_{1,z} = 1/2 \sum_n (f_n^{\uparrow\uparrow} + f_n^{\downarrow\downarrow})\zeta_n(t)$ , where  $\zeta_n(t) = \cos(\epsilon_n t) - i \sin(\epsilon_n t) \tanh(\epsilon_n/2T)$ , and we define  $f_n^{\sigma\sigma'} \equiv \sum_\lambda [u_{n,\lambda,K}^\sigma v_{n,\lambda,K'}^{\sigma'*} + u_{n,\lambda,K'}^\sigma v_{n,\lambda,K}^{\sigma'*}]$  [15]. For structures such as ours where the direction of the exchange fields varies with position it is more insightful to align the quantization axis with the local field vector. This helps distinguish the long-range nature of the equal-spin triplet correlations ( $f_1$ ) from

the damped oscillatory behavior of the opposite-spin triplets ( $f_0$ ). This is achieved by performing the appropriate spin rotations [14]. For the orientations considered here, the rotated amplitudes are  $f_0^{L,R} = 1/2 \sum_n \{\cos \theta_{L,R} (f_n^{\uparrow\uparrow} + f_n^{\downarrow\downarrow}) + i(f_n^{\uparrow\downarrow} - f_n^{\downarrow\uparrow})\}\zeta_n(t)$  and  $f_1^{L,R} = 1/2 \sum_n \{\sin \theta_{L,R} (f_n^{\uparrow\uparrow} + f_n^{\downarrow\downarrow}) + i(f_n^{\uparrow\downarrow} - f_n^{\downarrow\uparrow})\}\zeta_n(t)$ , where one sets  $\theta \equiv \theta_L$  on the left side and  $\theta_R = 0$  for the right side. The singlet pair amplitude is of course invariant under these rotations. When the exchange fields lie along one of the coordinate axes, the *singlet* pair amplitude depends only on whether the relative exchange field orientations are parallel, antiparallel, or perpendicular to each other [14]. The self-consistent methods used are extensions of those previously published [12] but now the matrix dimensions involved are doubled by inclusion of the spin degree of freedom.

**Results.**— As stated above, we assume that the exchange fields have the same magnitude,  $h$  (see Fig. 1), and lie in the plane of the graphene ( $\varphi_{L,R} = 90^\circ$  and  $\theta_R = 0^\circ$ ). Thus the exchange field orientation is described by the angle  $\theta_L \equiv \theta$  which can be manipulated by the transfer of spin angular momentum from injected electrons or by an external magnetic field. All spatial quantities are scaled by the Fermi wavevector,  $k_{FS} \equiv \mu_S/v_{FS}$ . We take  $d_F$  and  $d_S$  to be the same and (in scaled units) to equal the dimensionless SC coherence length:  $k_F \xi_0 = 100$ , where  $\xi_0 = v_{FS}/\Delta_0$ . Thus, in the figures the S region lies in the range 200–300 when spatially dependent quantities are shown. In the results that follow,  $h$  is normalized by  $\mu_S$  and we consider the ratio  $\tilde{\mu}_F \equiv \mu_F/\mu_S$  when describing the relative Fermi levels.

Figure 2 displays the gate voltage switching effect. The critical temperature,  $T_c$ , (computed by generalizing the methods of Ref. [12] and normalized to its value in a pure S sample) of the system is plotted in panel (a) as a function of Fermi level shift for various values of the exchange field. The results in this panel correspond to a perpendicular ( $\theta = 90^\circ$ ) configuration. As can be seen,  $T_c$  is nonmonotonic: it is largest when  $\tilde{\mu}_F$  is near  $-h/\mu_S$ . At larger values of  $\tilde{\mu}_F$ ,  $T_c$  decreases sharply: for  $T \gtrsim T_c$ , increases in  $\tilde{\mu}_F$  at constant  $\theta$  and  $h/\mu_S$  switch the system from SC to normal. When  $|\mu_F| \gg h$ , superconductivity becomes less dependent on the exchange field as evidenced by the coalescing of the curves for larger negative values of  $\tilde{\mu}_F$ : the proximity effects diminish due to the extreme mismatch in Fermi levels, resulting in greater isolation of the three regions.  $T_c$ , in turn is weakly dependent on both  $h$  and  $\mu_F$ . This behavior is also found for large positive  $\tilde{\mu}_F$  (not shown). For moderate  $\tilde{\mu}_F$ , the self-consistent proximity effects become even more important as the pair-breaking ferromagnet regions strongly reduce the SC correlations, resulting in the observed decline in  $T_c$  towards zero. This nontrivial behavior is further influenced by the shifting of the Dirac points by the exchange field, causing a corresponding shift in the peaks of each of the four curves in Fig. 2(a). These features are absent in standard metals, which lack tunable Fermi surfaces. The degree to which superconductivity can be tuned via  $\tilde{\mu}_F$  depends on the magnetic configuration of the system. We show in panel (b), the antiparallel field configura-

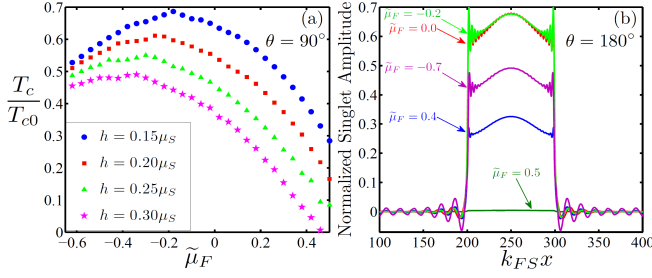


FIG. 2. (Color online) (a): Critical temperature  $T_c$  (normalized by its bulk value  $T_{c0}$ ) vs. the magnet doping parameter  $\tilde{\mu}_F$  for various values of  $h/\mu_S$  with  $\theta = 90^\circ$  (orthogonal exchange fields). In (b) the singlet pair amplitude at  $T/T_{c0} = 0.29$  is shown as a function of position, for an exchange field  $h/\mu_S = 0.2$ , and with  $\theta = 180^\circ$  (antiparallel exchange fields). Results for several  $\tilde{\mu}_F$  are shown.

tion,  $\theta = 180^\circ$ . There, the spatial profile of the self-consistent singlet pair amplitude (normalized to its value in a pure S sample) is shown at several values of  $\tilde{\mu}_F$ , at  $T/T_{c0} = 0.29$ . Just as for the  $T_c$  results in (a), we find nonmonotonic behavior in  $\tilde{\mu}_F$ : for  $\tilde{\mu}_F < -h/\mu_S$ , the singlet correlations are enhanced in the S region as the Fermi level shift increases. However if  $\tilde{\mu}_F$  is increased beyond about  $-h/\mu_S$ , SC correlations rapidly decrease and vanish as  $\tilde{\mu}_F$  reaches 0.5. Thus, by tuning the relative Fermi level of the F regions (e.g., by an electric field), the system will switch from a SC state to normal one (or vice versa) depending on the field configuration.

In Fig. 3 we exhibit the switching of superconductivity with orientation angle  $\theta$ . Panel (a) displays the normalized  $T_c$  vs.  $\theta$  at  $\tilde{\mu}_F = 0.5$ , for several values of  $h$ . For all four exchange fields shown,  $T_c$  increases monotonically as  $\theta$  goes from the parallel ( $\theta = 0^\circ$ ) to the antiparallel ( $\theta = 180^\circ$ ) configuration. Increasing the exchange field results in greater pair-breaking and thus an overall reduction in  $T_c$ . The curves are not related by a simple shift or factor, reflecting the nontrivial self-consistent nature of the solutions.  $T_c$  can be increased if one of the F layers is hole-doped while the other is electron-doped, but its sensitivity to  $\theta$  is much less. The greatest difference between the  $T_c$  values of parallel and antiparallel states occurs here for intermediate  $h \approx 0.2\mu_S$ . We also see from Fig. 3(a) that when  $\theta = 180^\circ$  and  $h = 0.2\mu_S$ ,  $T_c/T_{c0} \approx 0.28$ , which is consistent with Fig. 2(b), where at  $T/T_{c0} = 0.29$ , and  $\tilde{\mu}_F = 0.5$ , the system is slightly above  $T_c$ .

If  $T$  is just above the minimum in the  $T_c$  vs.  $\theta$  curves, superconductivity can be switched on by increasing  $\theta$ . The angular dependence of  $T_c$  found here is consistent with recent experimental and theoretical observed trends in 3D metallic F/S/F trilayers [16]. Panel (b) demonstrates the spatial dependence of the zero temperature self-consistent singlet pair amplitude for a representative set of field orientations. The behavior of this amplitude in the F regions reflects the characteristic damped oscillations arising from the spin splitting effects of the magnetism. As  $\theta$  decreases, superconductivity declines dramatically showing again that by controlling the field orientation, it can be switched on or off. Thus, Figs. 2 and

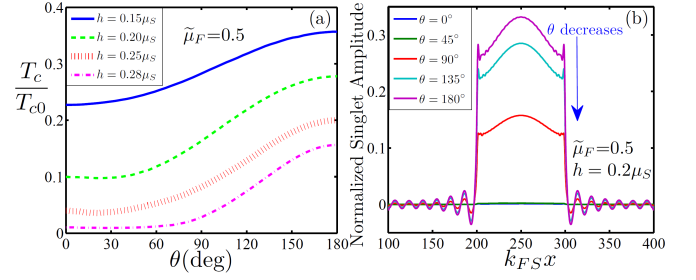


FIG. 3. (Color online) (a): Critical temperature versus the relative field angle  $\theta$  at several exchange fields,  $h/\mu_S$ . The doping parameter  $\tilde{\mu}_F$  is fixed at  $\tilde{\mu}_F = 0.5$ . In (b) we show the singlet pair amplitude normalized to its bulk value for different field orientations,  $\theta$  (see legend).  $T$  is set at  $T/T_{c0} = 0.12$ , and  $\tilde{\mu}_F = 0.5$ .

3 describe a graphene-based F/S/F nanostructure with normal to SC switching induced by variation of either relative field orientation or of the Fermi level of the F regions. If we consider opposite Fermi level shifts in the FM regions i.e.  $\mu_{FL} = -\mu_{FR}$ , we find that the observed switching phenomena disappear [14].

We now proceed to discuss the induced triplet pairs, which generate appreciable spin-valve effects in these junctions. Since the triplet amplitudes are odd in time, we must consider finite relative time differences,  $t$ , in the triplet correlation functions. We scale  $t$  by the “Debye” energy,  $\omega_D$ , and choose  $\omega_D t = 4.0$  as a representative value to discuss the behavior of the triplet amplitudes. We focus on moderately magnetic materials and set  $h/\mu_S = 0.2$ . The most interesting triplet amplitudes are those with nonzero spin projection on the quantization axis. Figure 4 illustrates the spatial dependence of these spin-triplet correlations in S. In panels (a) and (b) we plot respectively the real and imaginary parts of the equal-spin triplet amplitude  $f_1$  in the S region for several values of  $\tilde{\mu}_F$ . Both parallel,  $\theta = 0^\circ$ , and perpendicular,  $\theta = 90^\circ$ , relative exchange field orientations are included. These plots show that the equal-spin triplets more readily populate S when both magnets are in the parallel state ( $\theta = 0^\circ$ ). For a given  $\theta$ , the scale of the triplet correlations in S is then governed by the tunable Fermi shift in the F regions. We have found that on the other hand, in the F regions, the triplet amplitudes with zero spin projection (on the local quantization axis),  $f_0$ , are spatially characterized by the usual damped oscillatory behavior, similar to that of the ordinary singlet amplitudes.

The contrast between the spatial behavior of  $f_0$  and  $f_1$  in the F and S regions is best seen by comparing Figs. 4 and 5. In Fig. 5, panels (a) and (b) display respectively the imaginary part of  $f_1$  in F and the real part of  $f_0$  in S, for several values of  $\theta$  at  $\tilde{\mu}_S = -0.2$ . Panel (a) shows that  $f_1$  is long ranged in F and, when the relative exchange fields are non-collinear, it pervades the entire magnet region. One also sees, in panel (b), that the opposite-spin triplets are small and short ranged in the S region, also vanishing at  $\theta = 0^\circ$ , and  $180^\circ$ . In contrast, panels (a) and (b) in Fig. 4 illustrate non-vanishing equal-spin correlations in S at the same value of  $\tilde{\mu}_S$ . Thus



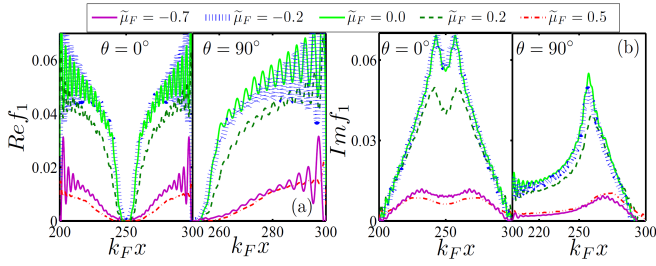


FIG. 4. (Color online) Triplet spin valve effect. In panels (a) and (b), respectively, we plot the real and imaginary parts of the equal-spin triplet correlations,  $f_1$ , in the S region. The curves in each of the panels represents a different doping level  $\tilde{\mu}_F$  in the F regions: by tuning  $\tilde{\mu}_F$ , the degree of equal-spin correlations in the superconductor can be controlled. The two relative exchange field orientations studied correspond to when the internal exchange fields are parallel ( $\theta = 0^\circ$ ) or perpendicular ( $\theta = 90^\circ$ )

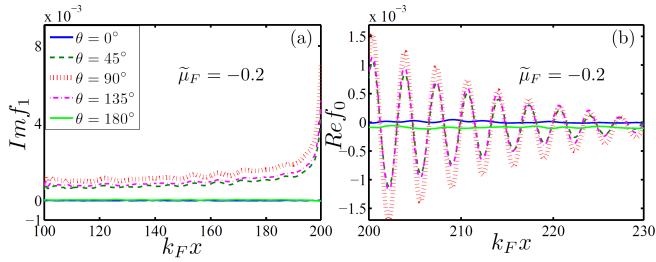


FIG. 5. (Color online) The imaginary part of  $f_1$  in F (panel (a)) and the real part of  $f_0$  in S (panel (b)) are plotted for multiple values of  $\theta$  and  $\tilde{\mu}_F = -0.2$ . (The corresponding imaginary and real parts vanish). The long range nature of  $f_1$  in F is seen in panel (a) while the obvious contrast between the long- and short-ranged nature of the equal- and opposite-spin triplets ( $f_1$  and  $f_0$ ) in S is seen by comparing panel (b) with Fig. 4.

the graphene-based F/S/F nanostructure can be utilized as a triplet spin valve. To achieve this equal-spin triplet spin valve effect, at least one of the ferromagnets should have a component of its magnetization out-of-plane. More important, the triplet spin switching aspect of the system can be experimentally achieved by modulating either the relative field orientation or the Fermi level [16]. This tuning is unavailable in ordinary materials.

**Conclusions.**— We have shown that F/S/F graphene nanostructures can exhibit very rich and experimentally accessible spin switching phenomena: For particular values of the relative field orientation of the two F regions, the induced equal-spin triplet correlations in the S region can be experimentally modulated in a controllable fashion by manipulating the Fermi level. This is in turn suggestive of a carbon-based spin-triplet transistor. Variations in relative field orientations or Fermi levels of the F regions allow the superconductivity to be switched on and off, thus producing a spin-controlled SC graphene switch. The results presented here are particular to the Dirac-like band structure in graphene, where, based on the magnetic configuration, the Fermi level can be shifted

in a controllable fashion (by doping or electric fields). They are also dependent upon the intrinsic 2D geometry, where the confining boundaries result in “relativistic” quantum interference effects not present in ordinary 3D metals. With recent experimental advances, including gate-tunable SC graphene hybrids [17], this work should stimulate future experiments involving graphene-based spin-switch devices. One possibility could involve magnetoresistance measurements for a sample configuration similar to that in Fig. 1, where the gate electrodes control the local Fermi level. The predicted spin-switch signatures should also be revealed in transport experiments via SC electrodes [18].

K.H. is supported in part by IARPA and a grant of HPC resources from the DOD HPCMP. O.T.V. thanks IARPA for grant N66001-12-1-2023. M.A. thanks J. Linder and T. Yokoyama for valuable discussions.

\* klaus.halterman@navy.mil

† otvalls@umn.edu; Also at Minnesota Supercomputer Institute, University of Minnesota, Minneapolis, Minnesota 55455

‡ phymalidoust@gmail.com; Also at Department of Physics, Faculty of Sciences, University of Isfahan, Hezar Jerib Ave, Isfahan 81746-73441, Iran

- [1] K. S. Novoselov *et al.*, *Science* **306**, 666 (2004); Y. Zhang *et al.*, *Nature (London)* **438**, 201 (2005); Y. W. Tan *et al.*, *Eur. Phys. J. Spec. Top.* **148**, 15 (2007); C.-H. Park *et al.*, *Eur. Phys. J. Spec. Top.* **148**, 15 (2007).
- [2] M. I. Katsnelson, *et al.*, *Eur. J. Phys.* **19**, 553 (1998).
- [3] Y.-W. Son, *et al.*, *Nature (London)* **444**, 347 (2006); N. Tombros, *et al.*, *Nature (London)* **448**, 571 (2007).
- [4] L. Vicarelli, *et al.*, *Nature Materials*, **11**, 865 (2012).
- [5] C. Berger, *et al.*, *Science* **312**, 1191 (2006); J. S. Bunch, *et al.*, *Nano Lett.* **5**, 287 (2005); J. S. Bunch, *et al.*, *Nano Lett.* **8**, 2458 (2008).
- [6] B. Soodchomshom, *et al.*, *Physica C* **468**, 1006 (2008); J. Linder, *et al.*, *Phys. Rev.* **B80**, 014513 (2009); M. Salehi, *et al.*, *J. Appl. Phys.* **107**, 123916 (2010).
- [7] J. Linder, *et al.*, *Phys. Rev.* **B82**, 041409(R) (2010).
- [8] Y. Asano, *et al.*, *Phys. Rev.* **B78**, 014514 (2008); Y. Hsu, *et al.*, *Phys. Rev.* **B81**, 045412 (2010); J. Wang, *et al.*, *Phys. Rev.* **B83**, 125425 (2011).
- [9] Q. Liang, *et al.*, *Phys. Rev. Lett.* **101**, 187002 (2008); A. G. Moghadam, *et al.*, *Phys. Rev.* **B78**, 115413 (2008).
- [10] D. Greenbaum, *et al.*, *Phys. Rev.* **B75**, 195437 (2007); Q. Zhang, *et al.*, *Phys. Rev. Lett.* **101**, 047005 (2008); W. Han, *et al.*, *Phys. Rev. Lett.* **105**, 167202 (2010).
- [11] J. Tworzydo, *et al.*, *Phys. Rev. Lett.* **96**, 246802 (2006); C. W. J. Beenakker, *Phys. Rev. Lett.* **97**, 067007 (2006); *Rev. Mod. Phys.* **80**, 1337 (2008); A. F. Morpurgo, *et al.*, *Phys. Rev. Lett.* **97**, 196804 (2006).
- [12] K. Halterman, *et al.*, *Phys. Rev.* **B84**, 064509 (2011).
- [13] M.V. Berry, *et al.*, *Proc. R. Soc. A* **412**, 53 (1987); P. Alberto, *et al.*, *Eur. J. Phys.* **17**, 19 (1996);
- [14] K. Halterman, O.T. Valls, M. Alidoust, in preparation.
- [15] K. Halterman, *et al.*, *Phys. Rev. Lett.* **99**, 127002 (2007).
- [16] J. Zhu, *et al.*, *Phys. Rev. Lett.* **105**, 207002 (2010).
- [17] B.M. Kessler, *et al.*, *Phys. Rev. Lett.* **104**, 047001 (2010).
- [18] H.B. Heersche, *et al.*, *Nature (London)* **446**, 56 (2007).